

UNIVERSIDAD DE NAVARRA

MASTER THESIS

High efficient Terahertz generation using pulse front tilt schemes

Author:

Paula ALCORTA

Supervisor:

Prof. Franz X.KÄRTNER

Dr. Santiago OLAIZOLA

*A thesis submitted in fulfilment of the requirements
for the degree of Master of Telecommunication Engineering*

in the

Optics Ultrafast and X-ray division

Tecnun

January 2015

Declaration of Authorship

I, Paula ALCORTA, declare that this thesis titled, 'High efficient Terahertz generation using pulse front tilt schemes' and the work presented in it are my own. I confirm that:

- This work was done wholly or mainly while in candidature for a research degree at this University.
- Where any part of this thesis has previously been submitted for a degree or any other qualification at this University or any other institution, this has been clearly stated.
- Where I have consulted the published work of others, this is always clearly attributed.
- Where I have quoted from the work of others, the source is always given. With the exception of such quotations, this thesis is entirely my own work.
- I have acknowledged all main sources of help.
- Where the thesis is based on work done by myself jointly with others, I have made clear exactly what was done by others and what I have contributed myself.

UNIVERSIDAD DE NAVARRA

Abstract

Engineering school

Tecnun

Master of Telecommunication Engineering

High efficient Terahertz generation using pulse front tilt schemes

by Paula ALCORTA

Intense ultrafast THz fields are of great interest for: electron acceleration, beam manipulation and measurement, and pump-probe experiments with coherent X-ray sources. Moreover, acceleration at THz frequencies has an advantage over RF, it can access high electric field gradients, and the beam delivery can be treated quasi-optically. This permits to reduce the size and cost of conventional accelerators and X-ray sources by many orders of magnitude. Nevertheless, high field THz pulse generation is needed.

Acknowledgements

First of all, I would like to thank Prof. Franz Kärtner for supervising and giving me the opportunity to do the master thesis on his group. His continual passion for science and unfailing optimism in the face of setbacks has been a mainstay in my scientific development. I would also like to thank my advisor Sergio Carbajo for all the time that he has dedicated to me, his wisdom and continuous help. I also want to thank Yago Olaizola for giving me the opportunity to do this master thesis and supervising my work from my home university.

I would like to express my gratitude to all those who helped and encouraged me during these months. I am grateful for the guidance of the members of the Terahertz group, Xiaojun Wu, Frederike Ahr, Jan Schulte and Ronny W. Huang. I am also thankful to my colleague, Miguel Arrieta for his constant help and long discussions, he has made a unique contribution to my work. I am indebted to Anne Laure Calendron and Hüseyin Cankaya who have been generous with their lab equipment and expertise. Finally, I have to thank Giovanni Cirimi, Giulio Maria Rossi, Yudong Yang, Roland Mainz, Luis E. Zapata, Kelly Zapata, Oliver Mücke, and Fabian Reichert for making the experience in CFEL unique and very special for me.

Finally, I would like to thank my family and friends for their continuous support during these months. This work would not have been possible without them.

Contents

Declaration of Authorship	1
Abstract	2
Acknowledgements	3
Contents	4
List of Figures	6
List of Tables	7
Abbreviations	8
Physical Constants	9
Symbols	10
1 Introduction	11
1.1 CFEL Centre for Free-Electron Laser Science	11
1.2 Efficient Terahertz (THz) generation: applications and motivation	12
1.3 Intrapulse difference frequency generation	13
1.4 Phase matching	14
1.4.1 Tilted Pulse Front (TPF) technique	14
1.4.2 Phase matching limitations	17
1.5 Conclusion	19
2 Pulse Front Tilt with congruent Lithium Niobate (cLN) at $1\mu\text{m}$	20
2.1 General experimental setup	20
2.2 Influence of the telescope	21
2.2.1 Correction of the input beam	21
2.2.2 Decoupling the sagittal and tangential plane focusing	22
2.3 Influence of the crystal temperature	23
2.4 Influence of the pulse duration	24
2.5 Intrinsic efficiency	28
2.6 Conclusion	31

3	Pulse Front Tilt with Lithium Tantalate (LT) at $1\mu\text{m}$	34
3.1	Benefits of using Lithium Tantalate	34
3.2	Design of the table setup	35
3.3	General experimental setup	36
3.4	Measurements and results	37
3.5	Conclusion	40
4	Conclusion	42
4.1	Conclusion and remarks	42
	Bibliography	44

List of Figures

1.1	(a) Energy level diagram for difference frequency generation. (b) Spectral diagram of intrapulse difference frequency generation (optical rectification). (c) Optical rectification of a broadband IR pulse yields a THz pulse with a spectrum spanning the few THz regime.	14
1.2	(a) Energy level of cascading. (b)-(f) Spectral picture of cascading.	15
1.3	Tilted pulse front scheme.	16
1.4	Phase matching from the angular dispersion point of view.	17
1.5	Phasor diagram for three different cases (a)phase-match, (b)moderate chirp, (c)phase mismatch.	18
2.1	Schematic of the PFT cLN setup.	21
2.2	Generalized cylindrical lens telescope in PFT setup.	22
2.3	Extracted conversion efficiency vs temperature.	23
2.4	Extracted conversion efficiency as a function of temperature for three different setups, with different optimum pulse durations.	25
2.5	Extracted THz energy as a function of temperature for three different setups, with different optimum pulse durations.	26
2.6	Extracted efficiency and THz energy as a function of pump energy, fluence, and peak intensity with a crystal temperature of 110K.	27
2.7	Relative extracted efficiency as a function of residual group-delay dispersion (GDD) from a grating-pair compressor for three independent setups with optimal operation points at different pump pulse durations.	28
2.8	Absolute spectral power of the input and red-shifted output pulses at different conversion efficiencies.	30
2.9	Absolute spectral power of the input and red-shifted output pulses at maximum 2% efficiency.	30
2.10	Focused THz beam with 0.73 and 0.83 mm FWHM tangential and sagittal diameters, respectively.	32
3.1	Schematic of the PFT LT setup.	37
3.2	Obtained THz energy, with a pulse duration of 0.7ps, as a function of energy at the crystal, fluence and peak intensity.	38
3.3	Extracted conversion efficiency, with a pulse duration of 0.7ps, as a function of energy at the crystal, fluence and peak intensity.	38
3.4	Extracted conversion efficiency, with a pulse duration of 1.7ps, as a function of energy at the crystal, fluence and peak intensity.	39
3.5	Measured output pump power spectra in logarithmic scale.	40

List of Tables

2.1	Extracted conversion efficiency, spectral bandwidth, center of mass, number of cascaded cycles, and intrinsic efficiency for different setups, optimized at different pulse durations.	31
3.1	Values of the constants of the Sellmeier's equation	35
3.2	Possible demagnification factors M that can be done using gratings with different number of lines.	35
3.3	Results of: center of mass, bandwidth, number of cycles, and intrinsic efficiency.	39

Abbreviations

OR	O ptical R ectification
PFT	P ulse F ront T ilt
THz	T era H ertz
LN	L ithium N iobate
LT	L ithium T antalate
AR	A nti R eflection
DFG	D ifference F requency G eneration
GDD	G roup D elay D ispersion
FCA	F ree C arrier A bsorption
TL	T ransform L imited
GVD	G roup V elocity D ispersion
FWHM	F ull W idth H alf M aximum
cLN	congruent L ithium N iobate
sLN	stoichiometric L ithium N iobate
cLT	congruent L ithium T antalate
TDS	T ime D omain S pectroscopy

Physical Constants

$$\text{Speed of Light } c = 2.997\,924\,58 \times 10^8 \text{ ms}^{-\text{S}} \text{ (exact)}$$

$$\text{Permittivity } \epsilon_0 = 8.85 \times 10^{-12} \text{ f/m}^{-\text{S}}$$

Symbols

s	distance	cm
E	energy	mJ
n	refraction index	
N	number of cycles	
k	wave vector	
f	focal length	cm
M	demagnification factor	
ω	IR frequency	Hz
Ω	THz frequency	Hz
λ	wavelength	m
η_i	Intrinsic efficiency	%
η	Extracted efficiency	%
γ	Pulse front tilt angle	degrees
α	Incident angle	degrees
ϕ	Diffraction angle	degrees

Chapter 1

Introduction

1.1 CFEL Centre for Free-Electron Laser Science

I have done this master thesis at the Center for Free-Electron Laser Science (CFEL), which is a novel joint enterprise of DESY, the Max Planck Society (MPG) , and the University of Hamburg. CFEL is designed to advance science with next generation light sources. The three partners join forces to explore structural changes of atoms, molecules, condensed, biological or warm dense matter on femtosecond time scales. I worked for the Ultrafast Optics and X-Rays division of Franz X.Kärtner.

The group develops novel table-top ultrafast light sources extending from the Terahertz (THz) through the x-ray wavelength range. We contribute enabling technologies for large-scale x-ray free- electron lasers, (XFELs) and we apply those sources in order to study ultrafast dynamical processes in matter.

Principal areas of research include femtosecond- to attosecond-precision timing distribution systems, and high-energy (joule) pulsed and high-average-power (kW) diffraction-limited laser amplifiers based on cryogenic composite thin-disk lasers.

These technologies are combined to produce multi-octave-wide high-energy lightwave synthesizers used in high-order harmonic generation, attosecond pulse generation, and coherent free-electron sources. In turn, these sources are applied to the study of field emission from nanophotonic and nanoplasmonic field-emitter arrays and to research in attosecond science [4]. In my case, I contributed in the high-efficiency, high-energy THz

generation group. In this chapter THz generation will be explained in detail. Moreover, in Chapter 2 the experiment applying the PFT technique using LN will be presented. Efficient THz generation will be addressed in detail, from an experimental point of view. Finally, in Chapter 3 an experiment using the PFT technique with a LT crystal will be presented. The main goal of this project is to obtain the maximum conversion efficiency.

1.2 Efficient Terahertz (THz) generation: applications and motivation

Terahertz(THz) radiation has a growing interest for applications such as study of molecules [5], charged particle acceleration [18, 19, 28], nonlinear spectroscopy [6, 17], high harmonic generation, medical applications [24], amongst others. As a consequence, there is a great need of the development of efficient strong-field THz sources.

Some of them require very high energy fields and are hampered by power scaling limitations. Most high power THz generation schemes depend on nonlinear frequency conversion from an optical laser [14, 25]. Therefore, extracting THz energy in the most efficient way is important in terms of laser scalability from a practical point of view. Nevertheless, we have to consider the practical limitations related to the scalability of lasers.

Optical rectification using pulse front tilts (PFT) has shown to be a promising technique for both high efficiency, and power scaling. Other techniques such as organic crystals are also promising in the few-THz frequency range [10, 22, 23, 26]. In the range between 0.1 to 1 THz, PFT has shown to be the most efficient method [8, 12]. Many groups are studying efficient THz generation theoretically and experimentally. Previous groups have proposed that efficiencies up to 10% are possible [7, 9]. However, experimentally, nobody has reported conversion efficiencies using the PFT technique exceeding the percent level [12]. Therefore, a revision of existing experimental approaches and theoretical models has to be done. In our group, we have shown that dispersion and cascading are the most limiting factors in efficiency scaling [21]. In Chapter 2 we will focus on how to find an experimental optima and back it up with the theory. Moreover, a good understanding of the role of the main limiting factors has enabled us to obtain the maximum extracted

conversion efficiency reported to date, 2%. This experimental value matches with the theoretical work presented in [21].

The goal of this master thesis is to present with experimental detail the power scaling mechanisms of THz generation via optical rectification from optical lasers. We will point towards the optimum conditions for maximum extracted conversion efficiency and find its limitations. In other words, we will explain the most crucial parameters and limiting factors to optimize a PFT setup. Then we will report the experimental results with a PFT congruent Lithium Niobate (cLN) setup and a PFT congruent Lithium Tantalate (cLT) setup.

1.3 Intrapulse difference frequency generation

First of all, we will explain some basic concepts about difference frequency generation (DFG). Those concepts explain the physical picture of the process that occurs in the experiments described in the following chapters. We will focus on the pulse front tilt (PFT) technique.

In difference frequency generation (DFG) a photon at an IR frequency ω mixes with a photon at a lower IR frequency $\omega - \Omega$ to generate a photon at the difference frequency Ω . The frequency Ω belongs to the THz spectral range, and there is another photon at $\omega - \Omega$ for energy conservation. An energy level diagram of the process that has been explained can be seen in Figure 1.1

Optical rectification can be seen as an intrapulse DFG process. The DFG occurs between all the frequency components of the broadband pulse. In Figure 1.1 it can be seen the process in the frequency domain. The bandwidth of the IR pump pulse determines the high frequency roll-off of the generated spectrum. The most important thing in optical rectification is that a single IR photon at ω can be down-converted more than once ($\omega \rightarrow \omega - \Omega \rightarrow \omega - 2\Omega \rightarrow \dots$) to generate multiple THz photons. The repetition of the downconversion phenomena is called cascading. An energy level diagram and a spectral diagram of cascading can be seen in Figure 1.2.

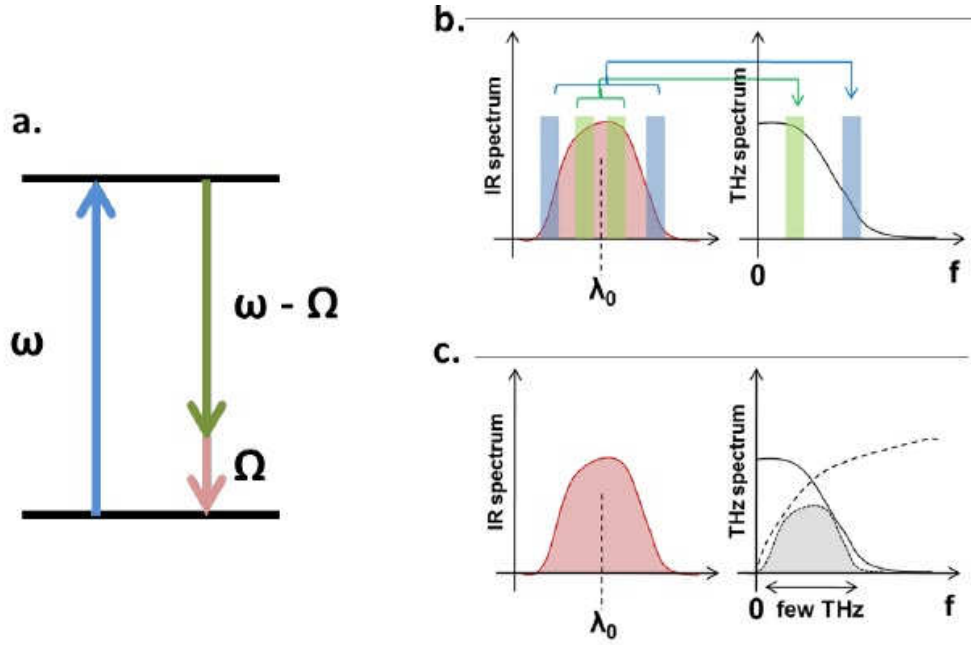


FIGURE 1.1: (a) Energy level diagram for difference frequency generation. (b) Spectral diagram of intrapulse difference frequency generation (optical rectification). (c) Optical rectification of a broadband IR pulse yields a THz pulse with a spectrum spanning the few THz regime.

1.4 Phase matching

The most important thing to generate THz with a high nonlinear conversion efficiency is phase matching. Due to the fact that the pump and THz velocities are highly mismatched, phase matching is a key issue. So, in this section we will explain the tilted pulse front technique, in order to satisfy the phase matching condition.

1.4.1 Tilted Pulse Front (TPF) technique

The driving nonlinear polarization is larger when the phase mismatch Δk is minimized. Δk can be written as:

$$\begin{aligned}
 \Delta k(\Omega) &= k(\Omega) + k(\omega) - k(\omega + \Omega) \\
 &\approx k(\Omega) - \Omega \left. \frac{dk}{d\omega} \right|_{\omega_0} \\
 &= \frac{\Omega}{c} [n(\Omega) - n_g(\omega_0)]
 \end{aligned} \tag{1.1}$$

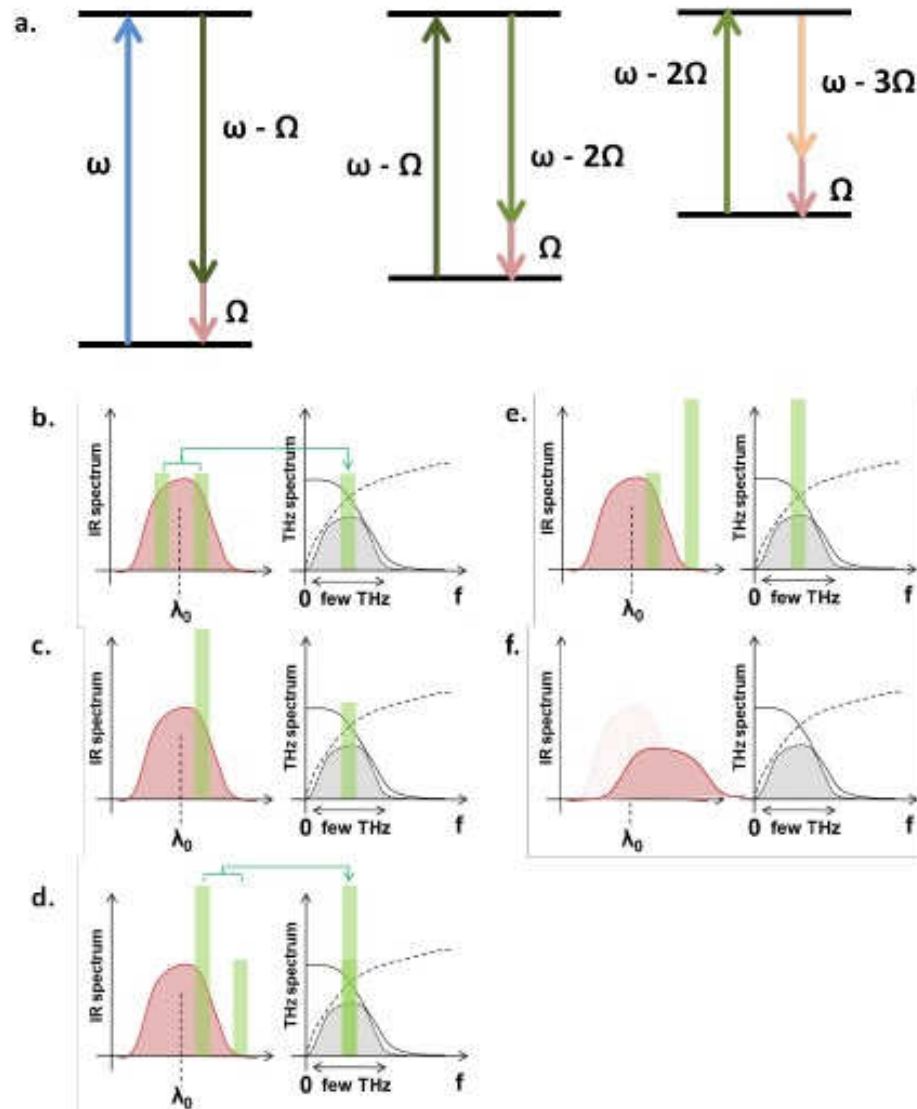


FIGURE 1.2: (a) Energy level of cascading. (b)-(f) Spectral picture of cascading.

This equation has been written under the assumption that $\Omega \ll \omega_0$, where ω_0 is the center of frequency of the IR pulse and Ω is the THz frequency. Equation 1.1 shows that the phase mismatch is proportional to the difference between the phase index of the THz and the group index of the IR. For the case of the LN, the difference between them is large, and as a consequence, the coherence length inside the crystal is short. In the next chapter it will be explained how to increase the coherence length (L) in the crystal in order to generate THz more efficiently.

Moreover, to reduce the phase mismatch we will use a noncollinear geometry phase-matching geometry. This geometry will be achieved using the Tilted Pulse Front technique shown in Figure 1.3

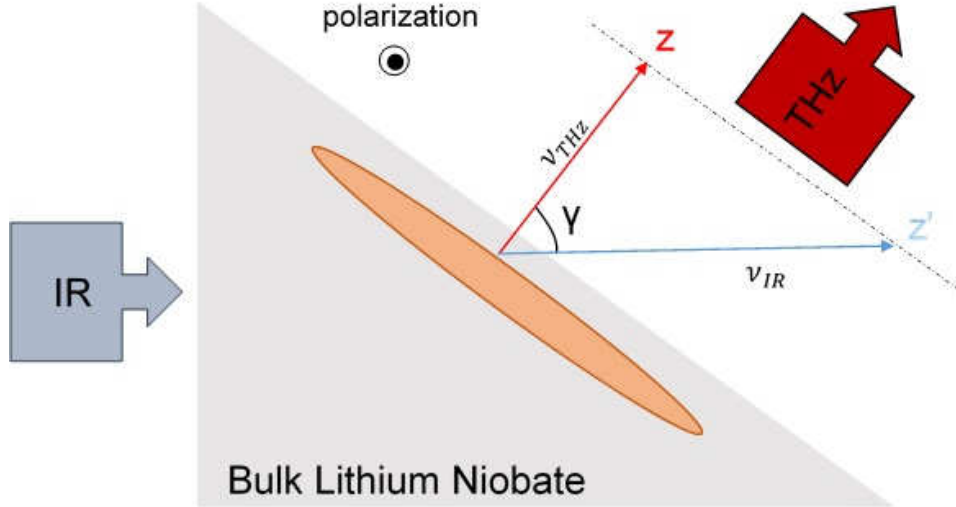


FIGURE 1.3: Tilted pulse front scheme.

The PFT technique consists on tilting the incident IR beam [11], that is propagating through the z -direction, with respect to its propagation direction by an angle γ . The angle γ is given by:

$$\cos(\gamma) = \frac{n_g(\omega_0)}{n(\Omega)} \quad (1.2)$$

The generated THz propagates in the z -direction, which is normal to the tilted pulse front. The phase mismatch follows the Equation 1.3

$$\Delta k \approx \frac{\Omega}{c} \left[n(\Omega) - \frac{n_g(\omega_0)}{\cos(\gamma)} \right] = 0 \quad (1.3)$$

The physical explanation is that the velocity of the pump projected in the direction of its pulse front is matched with the velocity of the THz wave.

The tilted pulse front is created by inducing angular dispersion onto the IR beam. It has been shown [11] that the pulse front tilt angle γ induced by an angular dispersion is given by:

$$\tan(\gamma) = \frac{n(\omega)}{n_g(\omega)} \lambda \frac{d\theta}{d\lambda} \quad (1.4)$$

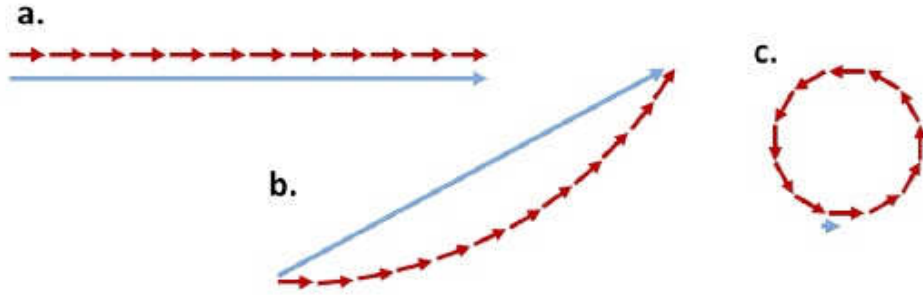


FIGURE 1.5: Phasor diagram for three different cases (a) phase-match, (b) moderate chirp, (c) phase mismatch.

In the case of fulfillment of the phase matching condition, the integral of the Equation 1.5 can be rewritten as:

$$\begin{aligned}
 |A(\omega + \Omega)||A^*(\omega)|e^{j[k(\omega+\Omega)-k(\omega)]z} &= |A(\omega + \Omega)||A^*(\omega)|e^{j\left[\frac{dk}{d\omega}\Big|_{\omega+\Omega}(\omega+\Omega)-\frac{dk}{d\omega}\Big|_{\omega}(\omega)\right]z} \\
 &= |A(\omega + \Omega)||A^*(\omega)|e^{j\left[\frac{d^2k}{d\omega^2}\Big|_{\omega}\Omega^2+\frac{d^3k}{d\omega^3}\Big|_{\omega}\Omega^3+\dots\right]z} \\
 &= |A(\omega + \Omega)||A^*(\omega)|e^{j\Delta k_c(\omega,\Omega)z}
 \end{aligned} \tag{1.6}$$

where, $\Delta k_c(\omega, \Omega)$ is the phase mismatch between $\omega + \Omega$ and ω . Moreover, due to the chirp:

$$\Delta k_c(\omega, \Omega) = \frac{d^2k}{d\omega^2}\Big|_{\omega}\Omega^2 + \frac{d^3k}{d\omega^3}\Big|_{\omega}\Omega^3 + \dots \tag{1.7}$$

The effect of dispersion on efficient THz generation can be represented using phasor diagrams. Figure 1.5 shows three different cases, varying the dispersion. The red phasor represents the normalized integrand at different frequencies ω within the integral, the blue phasor represents the sum of the red phasors (i.e. nonlinear polarization).

Figure 1.5(a) represents the case with no dispersive effects. The red phasors are lined up leading to a long blue phasor, in other words, the nonlinear polarization is large. In Figure 1.5(b) dispersive effects have been included. The red phasors are misaligned because there is a frequency dependent phase $\Delta k_c(\omega, \Omega)$. So, the blue phasor has been shortened, i.e. the nonlinear polarization has been reduced. As the propagation distance

z increases, the frequency dependent mismatch is accentuated, and the angle between the red arrows increases. In Figure 1.5(c) the perfect mismatch is represented. There is a distance L_D where the blue arrow goes to zero. As a conclusion, in Figure 1.5 the physical limitation in coherence length caused by dispersive effects can be understood.

1.5 Conclusion

To summarize, intense THz pulses can be generated via OR from ultrashort laser pulses in media with high optical second order nonlinearity. These can be excited when the group velocity of the pump pulses in the medium (cLN, cLT) matches the phonon-polariton phase velocity. To meet this condition we tilted the pulse intensity from the pump so that the projection of its velocity in the propagating direction equals the velocity of the THz radiation [11].

Chapter 2

Pulse Front Tilt with congruent Lithium Niobate (cLN) at $1\mu\text{m}$

2.1 General experimental setup

We use a PFT pumped at $1\mu\text{m}$ and employ a cLN prism doped with 5.5% MgO (5.5% MgO:cLN) [27] and c-axis cut, as depicted in Figure 2.1. We choose cLN for scalability purposes although sLN has shown better photorefractive properties [29] that enhance THz generation. The pump laser consists of a mJ-level Yb:KYW regenerative amplifier at 1KHz repetition rate, 1030nm of central wavelength and 2.6nm of spectral bandwidth with compressed pulses as short as 0.75ps FWHM Gaussian [3]. The pulses can be stretched up to a pulse duration equals to 6.71 ps and 4.21 ps. It corresponds to a dispersion of $-1.8 \cdot 10^6 fs^2$ to $1.12 \cdot 10^6 fs^2$ respectively. For these experiments we used a maximum energy of 4mJ. The pulse front was tilted to 63° using a grating with 1500 lines/mm, with a 93% efficiency. The incident angle to the grating has a value of $\alpha = 56.16^\circ$ and the diffraction angle is $\phi = 45.59^\circ$. We used a half-wave plate to rotate the polarization of the diffraction beam to s-polarization, parallel to the optical axis of the Lithium Niobate. For the imaging system we used two orthogonal cylindrical lenses. The first lens is a tangential lens with $f = 75\text{mm}$ and the second one is a sagittal lens with $f = 50\text{mm}$. The imaging system has a demagnification factor of approximately -0.5 in both axes, in order to decouple the tangential and sagittal imaging planes. The prism is a cLN prism doped with 5.5% MgO (5.5% MgO:cLN). The cLN prism measures

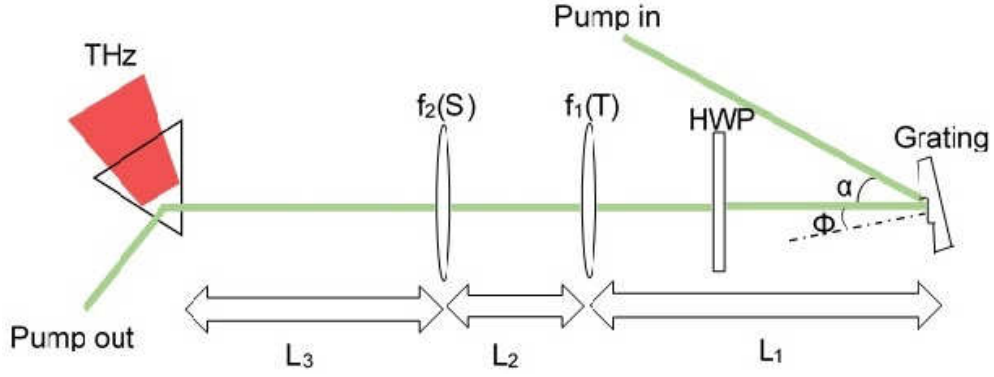


FIGURE 2.1: Schematic of the PFT cLN setup.

$57.9 \times 57.9 \times 54.4\text{mm}$ and has a apex angle of 63° . The crystal temperature is cooled down to cryogenic temperatures in a dewar. The temperature is monitored at its surface with a calibrated silicon sensor (Lakeshore DT471SD).

The prism has an anti-reflection (AR) coating with 49% enhancement. For the room temperature measurements there is a 1:1 imaging system after the cLN. For the imaging system we have used two TPX lenses with $f = 50\text{mm}$, onto an Ophyr pyrodetector. The pyroelectric detector is calibrated (Certificate No 716055-001). We also used a Spiricon Pyrocam IV after the THz lenses to obtain images of the THz beam. For the cryogenic measurements the imaging system was done using both TPX lenses as well as parabolic mirrors and onto the Ophyr pyroelectric detector.

2.2 Influence of the telescope

One of the biggest changes in the setup is to use cylindrical lenses on the telescope. Employing such geometry has two generalized advantages:

- Correction of the input beam
- Decoupling the sagittal and tangential plane focusing

2.2.1 Correction of the input beam

We moved the rotational angle of both tangential and sagittal lens to change the ellipticity of the beam. The lenses do not need to be orthogonal to each other. Thanks to

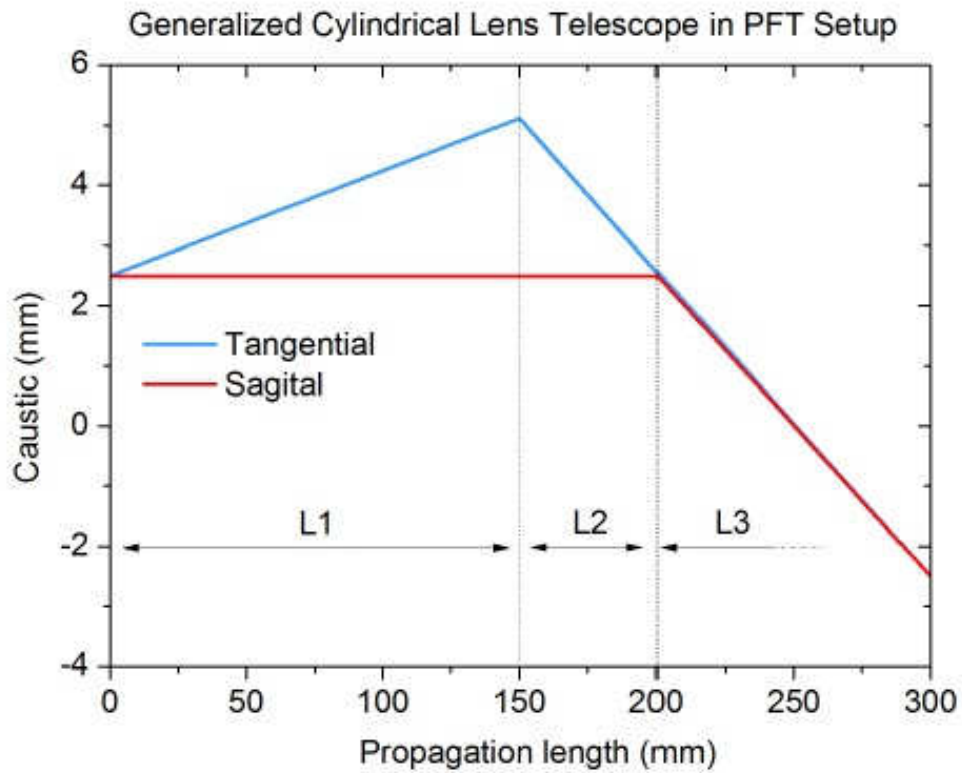


FIGURE 2.2: Generalized cylindrical lens telescope in PFT setup.

the rotation of the lenses we corrected astigmatism and ellipticity, which are inherent properties of any laser beam. So, we obtained the optimum beam shape and corrected the imperfections of the input beam profile.

2.2.2 Decoupling the sagittal and tangential plane focusing

The use of cylindrical lenses allows decoupling the tangential and sagittal plane focusing. The latter provides an additional degree of freedom in choosing the crystal location. We chose the optimal location of the crystal and found the balance between beam sagittal demagnification (i.e. fluence or peak intensity) and tangential demagnification (phase-matched PFT). It permits beam confinement in both axes. It is important to know that the tangential focusing is the one bound to the phase-matching. In Figure 2.2 it can be seen the corresponding beam caustic.

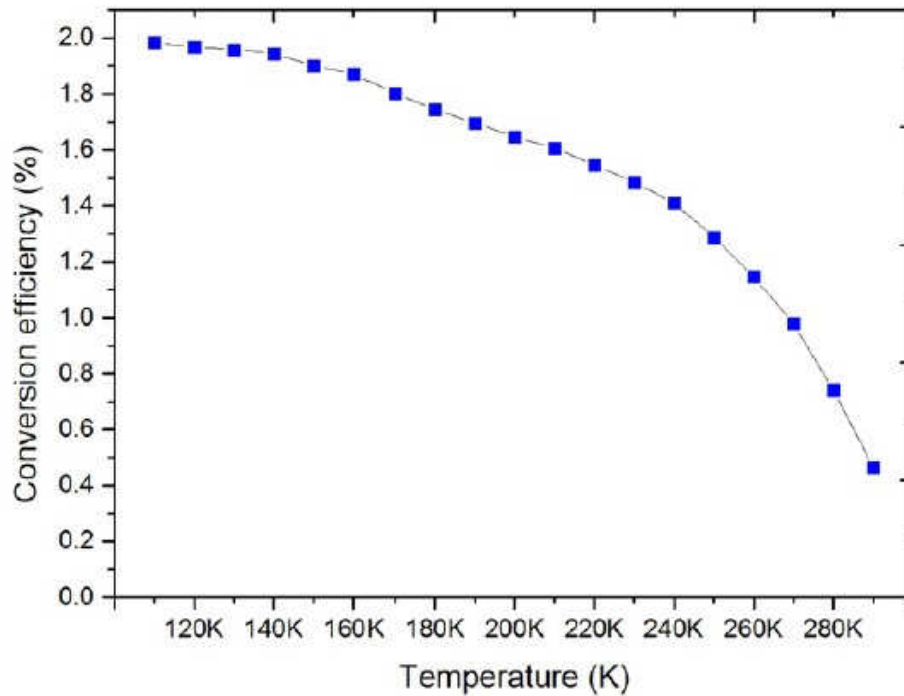


FIGURE 2.3: Extracted conversion efficiency vs temperature.

2.3 Influence of the crystal temperature

A major obstacle of THz generation in LN is the large absorption coefficient at room temperature. As thermal activation is thought to perturb the coherent interaction process, highly efficient generation of THz waves is expected at low temperature [13]. At room temperature the absorption arises from acoustic phonon resonant absorption. In the 0.1 to 1 THz range, only the lowest phonon frequency modes are excited in LN, and the absorption increases dramatically thereafter [1]. The THz absorption coefficient in LN at room temperature is of the order of 10-20 cm^{-1} [30, 31]. THz absorption severely depletes the extracted efficiency. On the other hand, cryogenically cooling reduces significantly the THz absorption. In fact, there is a three times higher stimulated Raman gain with the crystal cooled to 80K, due to the decrease in the bandwidth of the phonon mode [13]. At cryogenic cooling the absorption coefficient is an order of magnitude smaller [13]. As a consequence, with cryogenically cooling the crystal, both the optimal effective length in the crystal increases and so does the conversion efficiency. It is important to note that losses due to scattering from the photorefractive effect are still present at low temperatures, although their impact is not fully documented [16].

The temperature and its relation with the conversion efficiency can be seen in Figure 2.3. We obtained a record efficiency of 2% at 110K with a 1.12ps pulse duration. The measurement was acquired by maximizing the extracted conversion efficiency at 110K and then allowing the crystal to slowly thermalize up to room temperature. At cryogenic temperatures the absorption length is longer than at room temperature. So, optimizing the setup for the coldest point means that we allow the pump beam to travel a longer effective (L) before the cascaded broadening limits the process. The only parameter that varied was the temperature i.e. THz absorption. We used the same pump beam: energy, beam shape, spectrum and chirp. It has to be noted that at room temperature the THz absorption increases, and the optimum corresponds to a position of the crystal that corresponds to a smaller effective length (L') than at cryogenic temperatures. Therefore, at room temperature the efficiency that we obtain in these measurements is lower than the efficiency with the setup optimized for room temperature. The pump beam is traveling a nonlinear interaction distance that does not overcome the strong effect of THz absorption.

According to Figure 2.3 there is approximately a five fold increase in the extracted conversion efficiency from room temperature to 110K. The enhancement is more pronounced from 150K to room temperature. For temperatures lower than 150K, it does not saturate although the gain in efficiency increases marginally monotonically.

2.4 Influence of the pulse duration

The general consensus on optimal temporal shape of the pump pulse is that Fourier-limited pulses yield higher conversion efficiencies than temporally stretched ones [7]. A Fourier-limited optical pulse (or Transform-Limited pulse) is a pulse as short as its spectral bandwidth permits. In other words, its time–bandwidth product is as small as possible. In this Chapter, we show that the main influence of using Fourier-limited pulses is in the scaling of the peak intensity (for pulse durations not too far from TL). In fact, recent theoretical studies suggest that the peak THz frequency and corresponding efficiency can be tuned by adjusting the Fourier-limited pump pulse duration in the sub-ps range [9]. We have studied experimentally the influence of varying the pulse duration by introducing a negative chirp on the pump. We show that introducing group-delay dispersion (GDD) in the pump pulse of less than $10 \cdot 10^5 \text{ fs}^2$ corrects for alignment

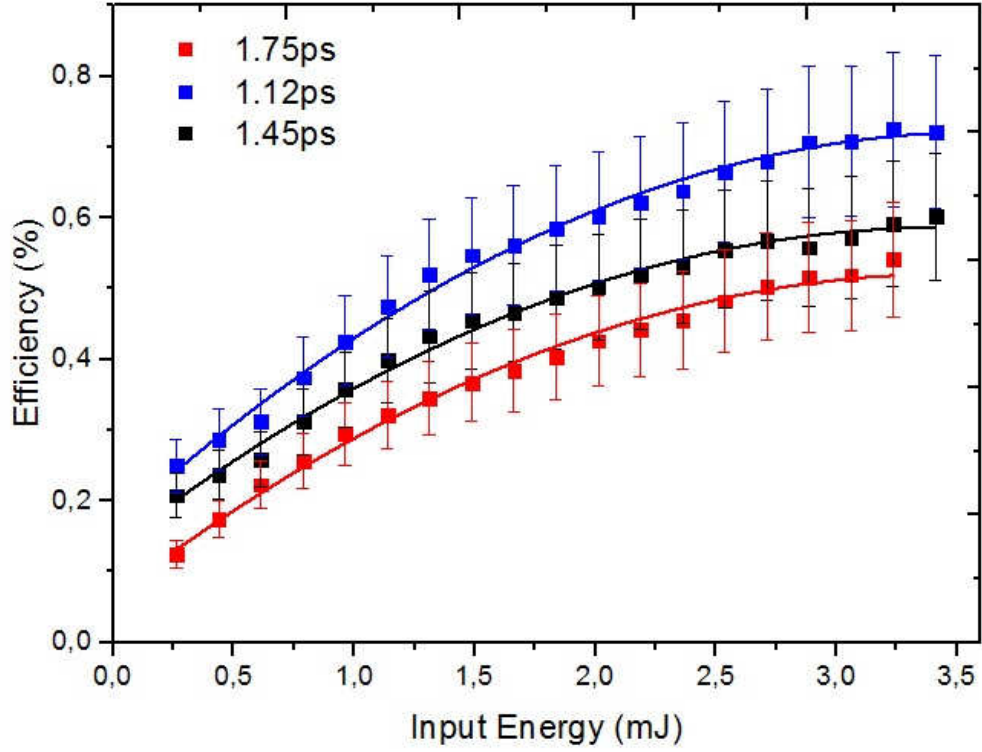


FIGURE 2.4: Extracted conversion efficiency as a function of temperature for three different setups, with different optimum pulse durations.

imperfections and optical aberrations and it therefore maximizes the effective length of the nonlinear interaction for THz generation.

The main effect of varying the temporal chirp of the pump pulse is the fine tuning of the PFT angle at the crystal without modifying the propagation axis of the beam. When a Fourier-limited pulse impinges a grating, the diffracted beam exhibits a PFT with an angle 2.1 and its spectral components are angularly dispersed.

$$\gamma_2 = \text{atan}(n_{opt} \cdot M \cdot \tan(\gamma)) \quad (2.1)$$

where, n_{opt} is the index of refraction, M is the demagnification factor and γ is the angle of the pulse front tilt. If we add temporal dispersion, some spectral components will arrive earlier at the nonlinear interaction point both, temporally and spatially. Therefore, it is a simple mechanism that allows varying the PFT angle at the expense of reducing the peak intensity. Nevertheless, the decrease in peak intensity does not necessarily imply a decline in extracted conversion efficiency since near-saturation operation can be achieved by modifying the pump fluence at the crystal.

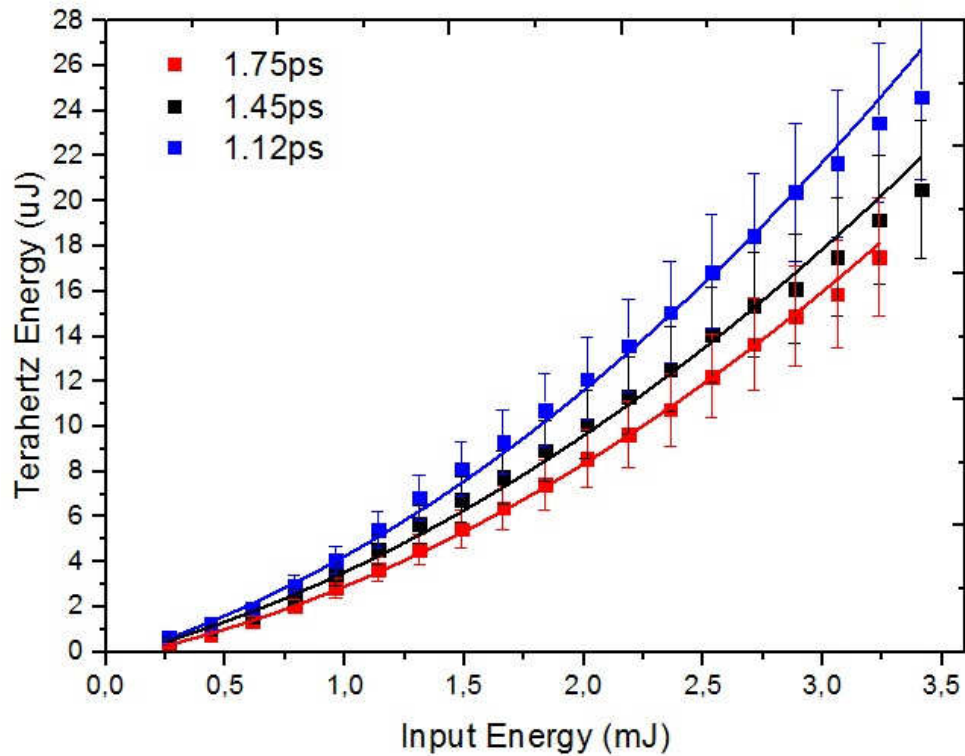


FIGURE 2.5: Extracted THz energy as a function of temperature for three different setups, with different optimum pulse durations.

In Figure 2.4 we can observe the obtained THz conversion efficiency as a function of temperature and in Figure 2.5 we can see the relationship between extracted THz energy and temperature. The three curves correspond to three different setups with three different stretched pulse durations and the same bandwidth. Adjusting the setup such that it would operate at its optimum with 1.45 ps and 1.12 ps pulse duration yields a steeper rise in the generated THz extracted energy. We can also observe that the curve saturates more rapidly for shorter pulse durations due to the stronger action of the photorefractive effect and free carrier absorption (FCA) through multi-photon absorption. It is important to note that the pulse duration is related to the damage threshold of the material. For longer pulse durations the damage threshold is lower. So, there is a limit in the negative chirp that can be introduced to optimize in the setup and compensate for misalignments. In other words, for long pulse durations the crystal can be damaged really easily. The importance of the damage threshold will be studied more in detail in the next chapter.

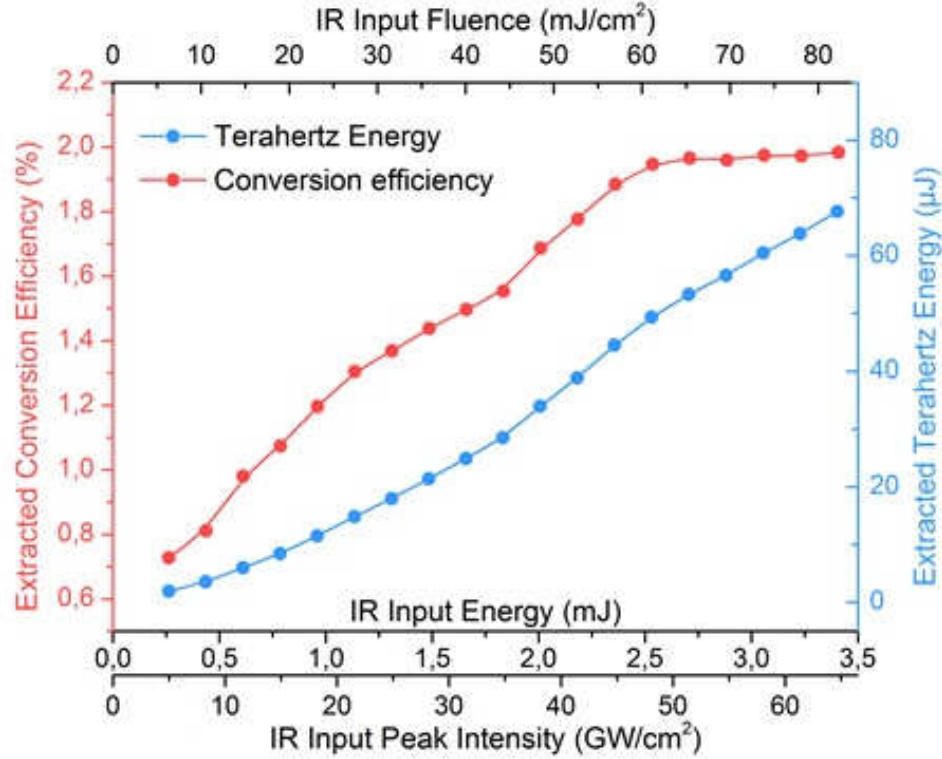


FIGURE 2.6: Extracted efficiency and THz energy as a function of pump energy, fluence, and peak intensity with a crystal temperature of 110K.

We concluded that there are multiple solutions to TPF OR in LN. For maximum extracted conversion efficiency, it is important to operate at an input fluence and intensity close to saturation. We find an optimal peak intensity operational point around $65\text{GW}/\text{cm}^2$ and extracted efficiency of 2 %.

Figure 2.6 shows the THz energy and conversion efficiency obtained for a pulse duration of 1.12 ps at 110K. The output energy curve in Figure 2.6 shows a quadratic behaviour with respect to the input intensity. The curve in Figure 2.6 exhibits a quadratic behaviour and it shows slightly saturation at around $65\text{GW}/\text{cm}^2$. Working with Fourier-limited pulses permits to increase the peak intensity, however the efficiency curve has a point of saturation. Therefore, it is helpful to work with negative chirped pulses to obtain high efficiencies before the saturation curve occurs.

In order to study the influence of the chirp in a TPF THz generation setup, the GDD relative to Transform limited (TL) pulses has been represented versus both, the normalized efficiency and the pulse duration (FWHM Gaussian). The GDD is introduced by varying the grating distance of the double-pass grating-pair compressor of the Yb:KYW regenerative amplifier. We used three different setups to study the influence of the chirp

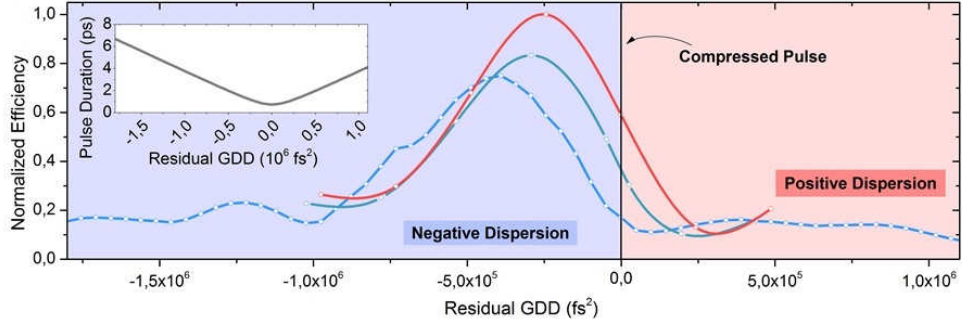


FIGURE 2.7: Relative extracted efficiency as a function of residual group-delay dispersion (GDD) from a grating-pair compressor for three independent setups with optimal operation points at different pump pulse durations.

with corresponding efficiencies peaking at three different points. We varied the grating compressor and introduced positive and negative chirp to obtain the extracted efficiency curve for every setup as a function of the GDD. The corresponding maxima are at 1.75 ps, 1.45 ps, and 1.12 ps, respectively. It can be observed that the introduction of negative chirp to the pulse helps to increase the extracted conversion efficiency.

We derive that the strong decline in efficiency with respect to GDD arises primarily from the phase-mismatch introduced by the variation of the PFT angle. This effect is dominant compared to a decrease in the peak intensity. So, it is important to note that there are multiple solutions to PFT OR in cLN. Therefore, input pulse duration can be a parameter, contrary to the general belief that Fourier-limited pulses are optimal [7].

2.5 Intrinsic efficiency

For validation purposes, we want to have an estimate of the value of the intrinsic efficiency. We refer to *extracted* efficiency as that coupled out of the cLN crystal, transported, and detected onto the detector. *Intrinsic* efficiency corresponds to the one generated in the crystal before it is absorbed, out-coupled, transported, and detected (i.e. the energy efficiency corresponding to the internal photon-to-photon conversion). On one hand, the number of cascading cycles (N), or the number of optical photons that are recycled after undergoing the nonlinear frequency down-conversion, increases cubically relative to the pump optical frequency and assists greatly in enhancing the photon-to-photon conversion (Manley-Rowe limit), since as the pump spectrum shifts

towards longer wavelengths it continues to transfer optical energy to the THz frequencies (Ω) as long as the phase mismatch is small. The effect of cascading can be seen in Figure 1.2

On the other hand, when the pulse front tilt is introduced to achieve achromatic frequency conversion, angular dispersion dominates the group-velocity dispersion (GVD) term (typically $|GVD_{ang}| > 1 \cdot 10^5 fs^2/mm$) against material dispersion ($|GVD_{mat}| \approx 250 fs^2/mm$) as:

$$GVD_{ang} \approx -\frac{n_{opt}}{\omega_0 \cdot c} \tan(\gamma)^2 \quad (2.2)$$

By up to two orders of magnitude, this limits the coherence length to a few millimeters and thus affects the conversion efficiency.

Measuring the broadened spectrum of the pump pulse after the nonlinear interaction may provide a quantitative estimate of the intrinsic conversion efficiency from the nominal cascading cycles. Moreover, a comparison between the extracted and intrinsic efficiencies may also provide information on how good the THz transport is.

For this purpose, we recorded the spectra of the pump pulse after the THz generation process as a function of extracted efficiency at room temperature for an optimized setup at different input energies. Figure 2.9 shows the broadening that experiences the spectrum due to high efficient THz generation at room temperature.

Let us focus on the most efficient case. There is a strong spectrum red-shift at the highest efficiency with frequency components reaching up to 1120 nm due to cascading effects, which means high efficient THz generation.

The center of mass is at 1057.7 nm and there is a bandwidth of 67.2 nm (calculated from the center of mass of the input spectrum). We can easily estimate the nominal number of cycles from:

$$N = \frac{c}{\nu_{THz}} \left(\frac{1}{\lambda_1} - \frac{1}{\lambda_2} \right) \quad (2.3)$$

Where, c is the speed of light, ν_{THz} is the peak THz frequency (300GHz), λ_1 is the center of mass of the input spectrum, and λ_2 is the center of mass of the output spectrum. In

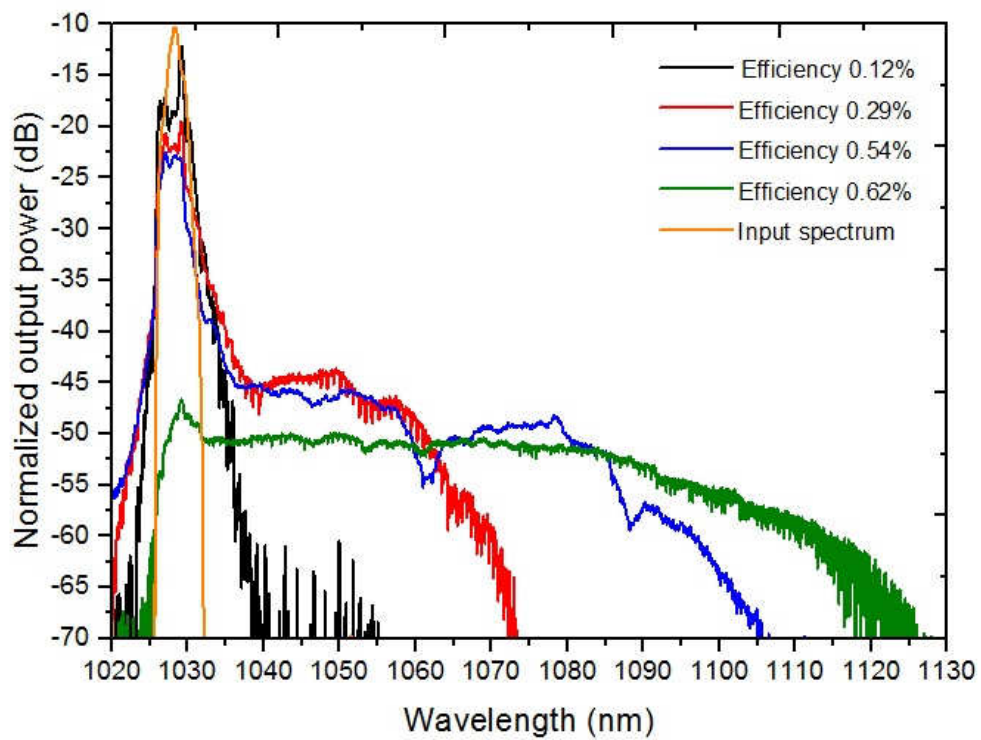


FIGURE 2.8: Absolute spectral power of the input and red-shifted output pulses at different conversion efficiencies.

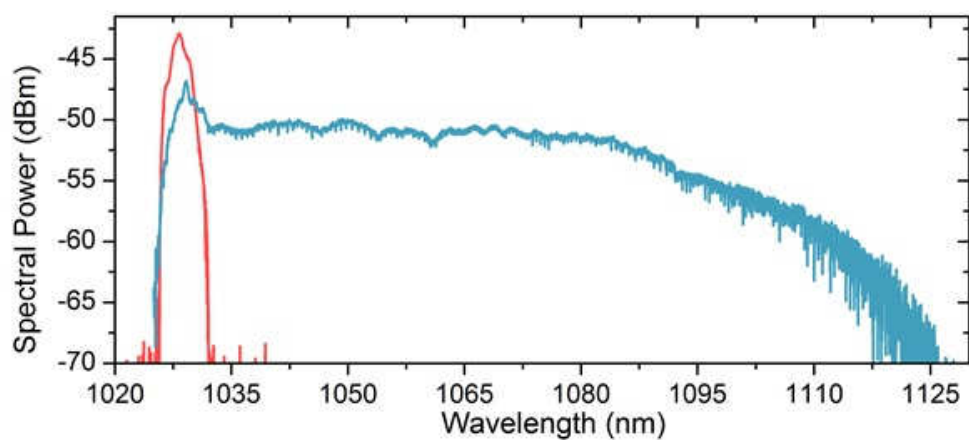


FIGURE 2.9: Absolute spectral power of the input and red-shifted output pulses at maximum 2% efficiency.

TABLE 2.1: Extracted conversion efficiency, spectral bandwidth, center of mass, number of cascaded cycles, and intrinsic efficiency for different setups, optimized at different pulse durations.

Extracted conversion efficiency (%)	Spectral bandwidth (nm)	Center of mass (nm)	Number of cycles	Intrinsic efficiency (%)
Input	2.38	1028.4	0	0
0.12	3.36	1028.9	2	0.21
0.29	5.95	1030.2	3	0.31
0.54	9.6	1033	6	0.62
0.72	67.2	1057.7	27	2.77

Table 2.1 we can observe the number of cycles N , bandwidth, and intrinsic efficiency for different pulse durations:

For this case, $N = 27$ cycles, and the corresponding intrinsic efficiency is $\eta_i = 2.77\%$. The 2% is the extracted conversion efficiency from the cryogenically cooling at the maximum broadening. So, the intrinsic efficiency $\eta_i = 2.77\%$ and the measured efficiency is $\eta = 2\%$. the difference between them is due to the out-coupling losses and the losses in the window of the cryogenic dewar. The cLN prism has anti-reflection (AR) coating to reduce the out-coupling losses and enhance a 30% the transmission. The width and material of the window of the cryogenic dewar can be taken into account to reduce the difference between intrinsic and extracted conversion efficiencies. In our case, there is a 0.77% difference between extracted and intrinsic efficiency. So, we conclude that the beam transport is good.

The use of cylindrical lenses also allows tailoring and improving the quality of the THz output beam. By optimizing not only the efficiency but also, the focusability of the THz beam, the performance of our setup grants electric fields with a value of $0.2GV/m$ with $68\mu J$ energy. The beam is nearly diffraction limited, with 1.24mm and 1.41mm ($1/e^2$) tangential and sagittal diameters, respectively, which suits strong-field THz applications.

2.6 Conclusion

In conclusion, we have investigated the most important tunable parameters in order to have an efficient THz generation setup:

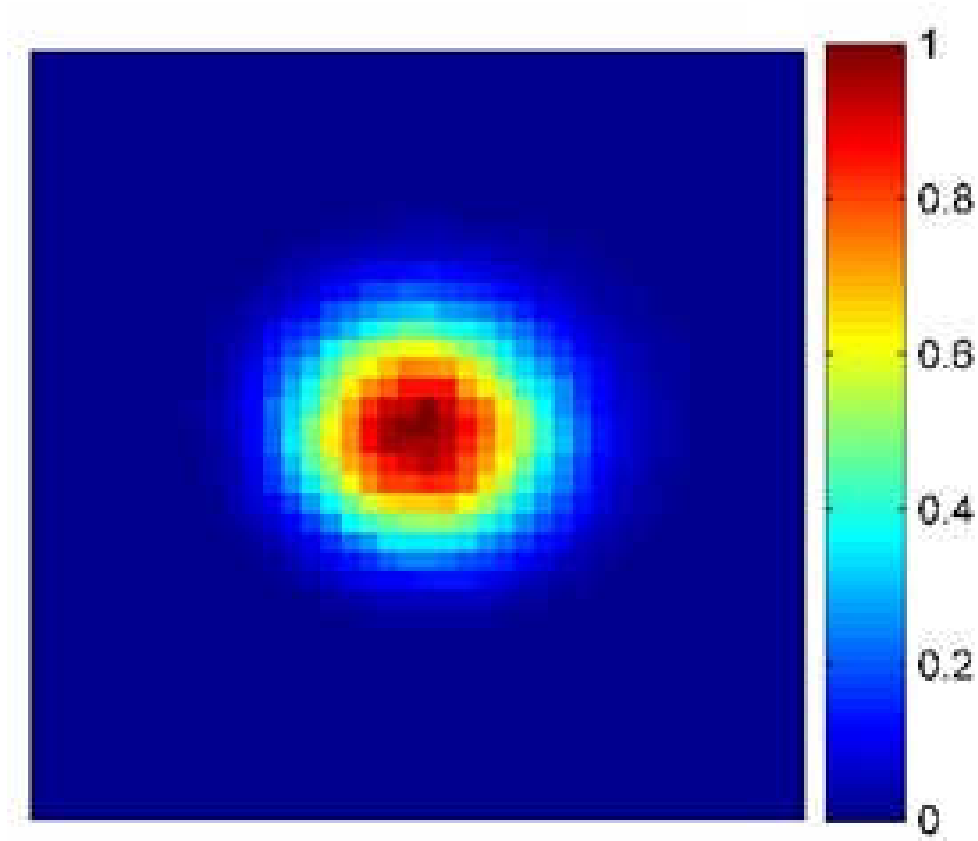


FIGURE 2.10: Focused THz beam with 0.73 and 0.83 mm FWHM tangential and sagittal diameters, respectively.

- The use of cylindrical lenses decouples the tangential and sagittal plane focusing. It also shows that imperfections in the beam profile can be corrected, and we achieve higher extracted conversion efficiency. It permits to custom shape the pump spatial distribution, in order to increase the quality of the THz pulses.
- The pulse duration is also a crucial tunable parameter. The introduction of negative chirp does fine tuning of the tilted pulse front and compensates the misalignments of the setup. We have exploited the spectral-temporal shape of the pump beam to its optimum.
- Due to the spatial and temporal tuning of the beam shape, we report a record 2% available THz conversion efficiency, close to the maximum theoretical limit, and an excellent beam quality, diffraction-limited.

It is possible to increase the extracted conversion efficiency using stoichiometric Lithium Niobate (sLN). cLN has higher absorption [20], and lower effective second order nonlinear coefficient d_{eff} [15], what makes sLN more suitable for efficient THz generation. sLN

has a higher nonlinear coefficient and decreased photorefractive effects. Therefore, it permits an improvement of 2% over the use of congruent Lithium Niobate. However, at the moment the fabrication process does not permit to grow sLN crystals as big as the cLN.

Currently, the performance of our setup grants electric fields as high as 0.2 GV/m and 68 μ J THz energy. The beam is focusable close to diffraction limit and it suits strong-field THz applications. In other words, these specifications suffice the requirements of a THz gun capable of accelerating electrons to the range of several keV from rest, or to accelerate non-relativistic electrons to relativistic speeds in accelerating structures. In addition, scaling the pump energy by using cryogenic Yb:YLF laser technology, THz operation regimes in the mJ-level and fields strengths of several GV/m are achievable. Therefore, it opens the possibility of direction acceleration of electrons in free space without the assistance of any additional structure or energy confinement method, and thus overcoming inhomogeneities and material limitations.

The content of this Chapter has been written in a paper and submitted to *Optica*.

Chapter 3

Pulse Front Tilt with Lithium Tantalate (LT) at $1\mu\text{m}$

3.1 Benefits of using Lithium Tantalate

In this chapter we will use a PFT pumped at $1\mu\text{m}$ employing a Lithium Tantalate prism. We choose cLT instead of cLN because it is a promising less studied crystal. The main considerations when using cLT with respect to cLN are:

- The main advantage is that the damage threshold is higher than other materials such as: Lithium Niobate, ZnTe or GaAs.
- The disadvantage is that the pulse front tilt angle needed to achieve the phase matching condition is higher, due to the fact that the THz index of refraction of the Lithium Tantalate is higher than the one for the Lithium Niobate.

However, the advantages and potential of the material makes it worth studying the extracted conversion efficiency that can be obtained. The main idea of the experiment is to focus the beams as much as possible, and increase the operational peak-intensity without damaging the materials of the components of the setup. Therefore, the high damage threshold of the Lithium Tantalate will be exploited.

TABLE 3.1: Values of the constants of the Sellmeier's equation

Constant	Value
A	4.514261
B	0.011901
C	0.110744
D	-0.02323
E	0.076144
F	0.195596
c(t)	$1.5662 \cdot 10^{-8}(T + 273.15)^2$

TABLE 3.2: Possible demagnification factors M that can be done using gratings with different number of lines.

Grating (lines/mm)	M = 1/3	M = 1/4	M = 1/5	M = 1/6	M = 1/7
600	✓	✓	✓	✓	✓
900	✓	✓	✓	✓	✗
1200	✓	✓	✗	✗	✗
1500	✓	✗	✗	✗	✗

3.2 Design of the table setup

Firstly, we calculated the pulse front tilt angle γ , using Equation 3.1, in order to fulfill the phase matching condition.

$$\cos\gamma = \frac{n_{opt}}{n_{THz}} \quad (3.1)$$

The value of n_{THz} has been calculated using the Sellmeier equation [2]:

$$n_e^2(\lambda, T) = A + \frac{B + b(t)}{\lambda^2 - [C + c(t)]^2} + \frac{E}{\lambda^2 - F^2} + \Delta\lambda^2 \quad (3.2)$$

where λ is in μ m, T in $^{\circ}$ C and the constants have the following values:

The main goal is to focus the beam as tight as possible. In order to do that we will calculate the incident angle α and the diffraction angle ϕ to the grating, varying both: the number of lines of the grating and the demagnification factor. In Table 3.2 it can be seen the possible demagnification factors using different gratings.

Once that both, the pulse front tilt angle γ and the demagnification factor M have been chosen the incidence angle α and diffraction angle ϕ will be calculated using the Equation 3.3, 3.4, and 3.5.

$$\gamma_2 = \text{atan}(n_{\text{opt}} \cdot M \cdot \tan(\gamma)) \quad (3.3)$$

$$\cos(\phi) = \frac{\lambda}{d \cdot \tan(\gamma_2)} \quad (3.4)$$

$$\sin(\alpha) = \frac{\lambda}{d} - \sin(\phi) \quad (3.5)$$

At this point we have fixed all the design free parameters and the setup can be implemented.

3.3 General experimental setup

We use a PFT pumped at 1 μ m and employ a cLT prism with no MgO doping, as depicted in Figure 3.1. The pump laser consists of a mJ-level Yb:KYW regenerative amplifier at 1KHz repetition rate, 1030nm of central wavelength and 2.6nm of spectral bandwidth [3]. The compressed pulses are as 0.75ps FWHM Gaussian. The pulses can be stretched up to 6.71ps and 4.21 ps, pulse duration. These values correspond to $-1.8 \cdot 10^6 f s^2$ to $1.12 \cdot 10^6 f s^2$ dispersion, respectively. For this experiment we used a maximum energy of 3mJ. The laser permits to use more energy, however for damage reasons we used a maximum of 3mJ. Using more than 3mJ of energy the grating was visibly damaged.

Moreover, the pulse front was tilted to 71 $^\circ$ using a grating with 1200 lines/mm, with a 75% efficiency. The incident angle to the grating has a value of $\alpha = 25.89^\circ$ and the diffraction angle is $\phi = 53.07^\circ$. We used a half-wave plate to rotate the polarization of the beam to s-polarization, parallel to the axis of the Lithium Tantalate.

Furthermore, we used two orthogonal cylindrical lenses for the imaging system. The first lens is a tangential lens with $f = 75\text{mm}$ and the second one is a sagittal lens with $f = -50\text{mm}$. The imaging system has a demagnification factor of approximately -0.33 in both axes. As shown in Chapter 2 the imaging system permits to decouple both the tangential and sagittal imaging planes.

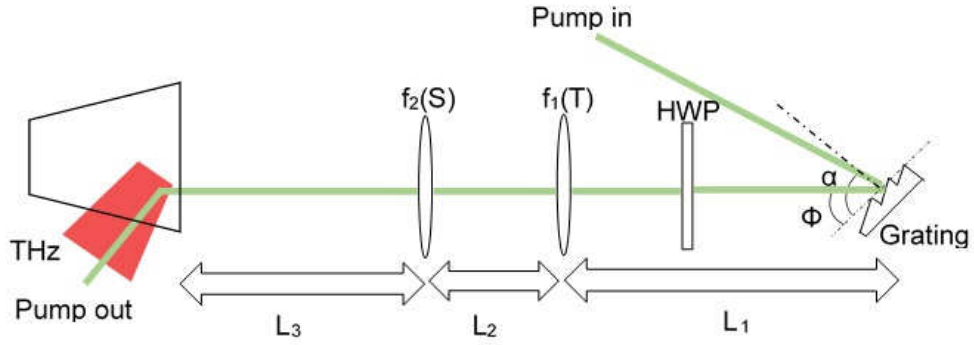


FIGURE 3.1: Schematic of the PFT LT setup.

The prism is $47.43 \times 47.15 \times 47.43 \text{mm}^3$, with a cut parallel to the side of the input beam. The cut does not affect the performance of the extracted conversion efficiency. However, it affects in the recording of the output spectrum.

Finally, the prism has an anti-reflection (AR) coating with 49% enhancement. The THz energy was measured using a Gentech pyrodetector.

3.4 Measurements and results

In Figure 3.2 we can see the obtained THz energy as a function of the energy at the crystal, fluence, and peak intensity. The behaviour of the curve is linear. The maximum value of THz energy that we have obtained is $1\mu\text{J}$ at a $80\text{GW}/\text{cm}^2$ peak intensity. The Lithium Tantalate has a higher damage threshold, of about an order of magnitude for sub-ps pulses, so we can increase the peak intensity by a factor of four. According to Figure 3.3 the value of the extracted conversion efficiency is around 0.05% and the curve has a quadratic behaviour, we can see a beginning of saturation at $60\text{GW}/\text{cm}^2$. Those measurements have been taken with a 0.7ps (TL FWHM Gauss) pulse duration.

In Chapter 2 we have seen that by introducing a negative chirp not only the setup can be optimized, but also we can see how far we are from the optimum pulse duration. So, the pulse duration has been modified and we can see an optimum at 1.7ps (FWHM). In Figure 3.4 it can be seen that the curve has also a quadratic behaviour, and the extracted conversion efficiency has slightly improved. However, it might be saturating at around $60\text{GW}/\text{cm}^2$.

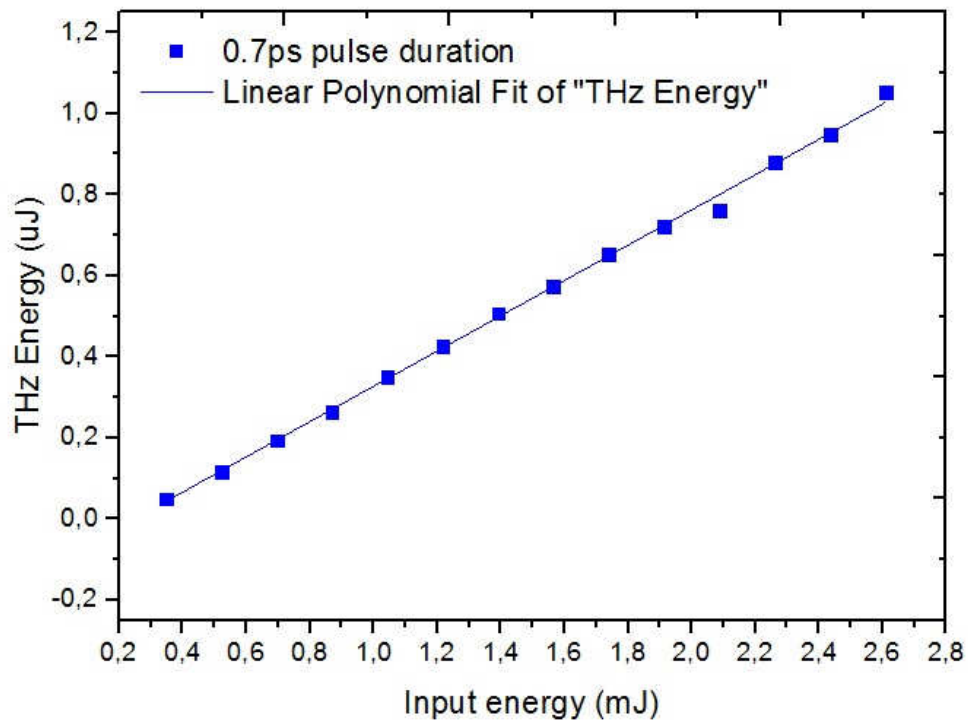


FIGURE 3.2: Obtained THz energy, with a pulse duration of 0.7ps, as a function of energy at the crystal, fluence and peak intensity.

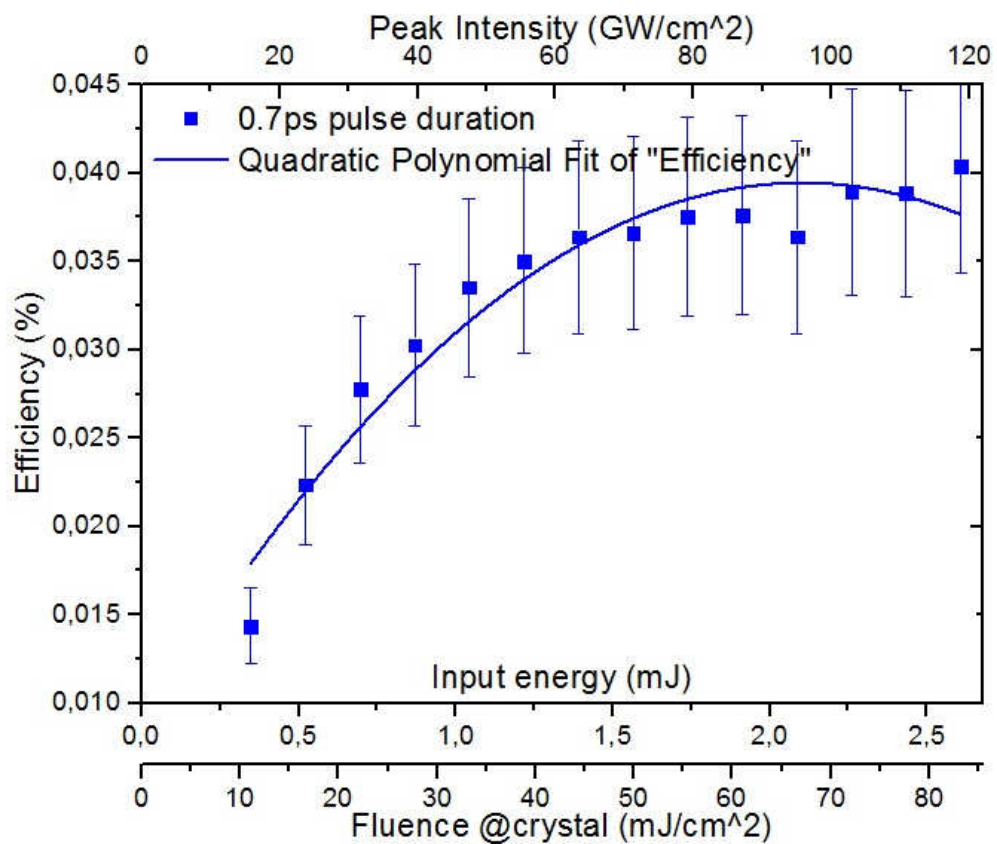


FIGURE 3.3: Extracted conversion efficiency, with a pulse duration of 0.7ps, as a function of energy at the crystal, fluence and peak intensity.

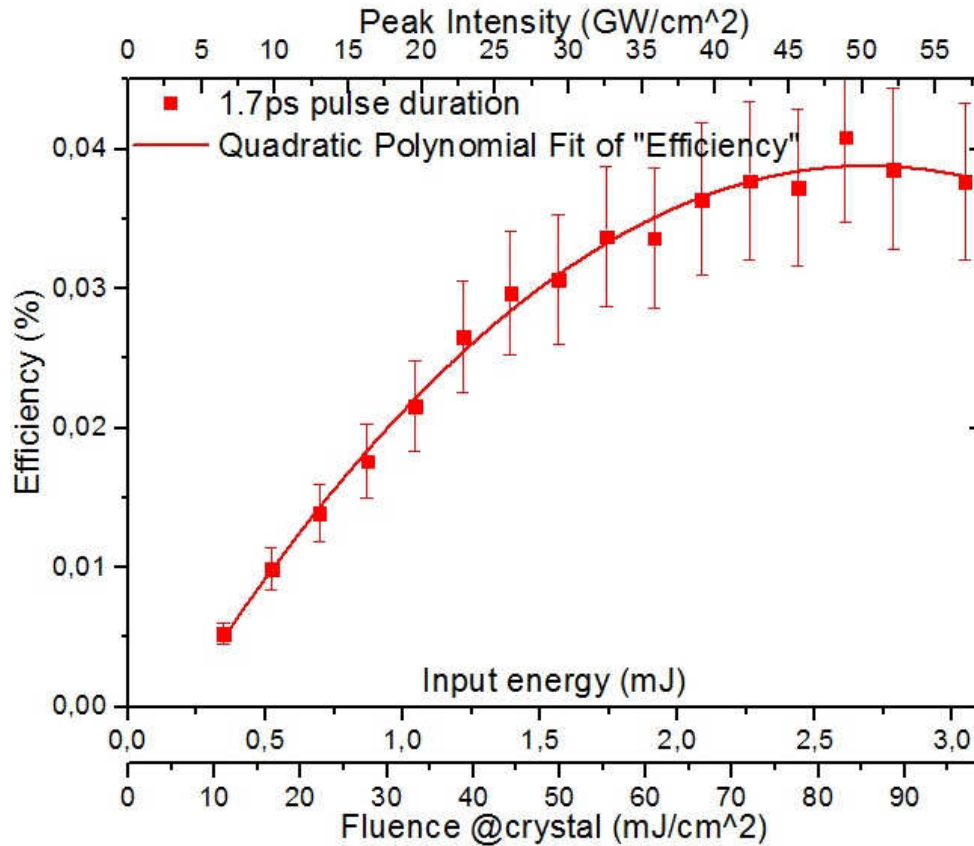


FIGURE 3.4: Extracted conversion efficiency, with a pulse duration of 1.7ps, as a function of energy at the crystal, fluence and peak intensity.

TABLE 3.3: Results of: center of mass, bandwidth, number of cycles, and intrinsic efficiency.

Center of mass (nm)	1029.9
Bandwidth (nm)	3.36
Number of cycles	3
Intrinsic efficiency (%)	0.31

We have taken the output spectrum to see how much broadening there is, due to efficient THz generation. Nevertheless, it is important to note that due to the shape of the crystal it is difficult to fully record the output spectrum. In Figure 3.5 we can observe both the input, and output spectrum in logarithmic scale. There is broadening up to 1050nm, however the drop is very large (-20dBm). What matches with the low efficiency value that has been calculated.

Finally, we will calculate the: center of mass, bandwidth, number of cycles, and intrinsic efficiency, as it has been done in Chapter 2. In Table 3.3 we can observe the results that we have obtained.

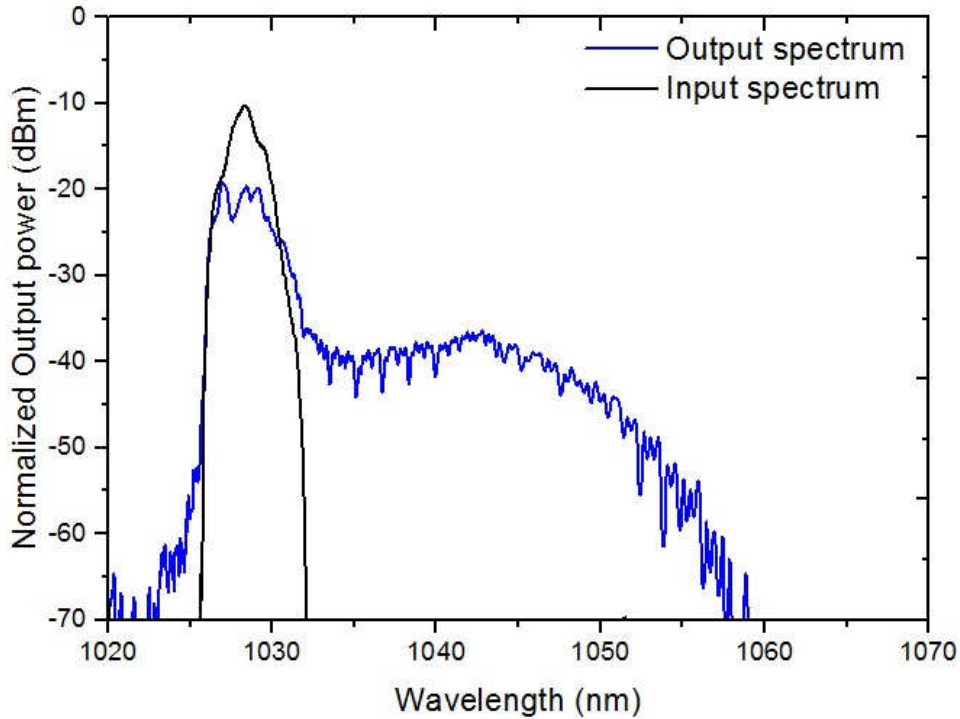


FIGURE 3.5: Measured output pump power spectra in logarithmic scale.

3.5 Conclusion

In conclusion, we have investigated the suitability of a cLT prism using the PFT technique at 1 μ m. The main objective was to focus the beam as much as possible, and exploit that cLT has a higher damage threshold than cLN. However, the value of the extracted conversion efficiency 0.05% is low. We are going to present the parameters that can be tuned to try to obtain if a higher efficiency can be achieved.

- Use another grating with a different number of lines, and change the design parameters. Another demagnification factor can be chosen with its corresponding incident angle α and diffraction angle ϕ . The maximum peak intensity that can be used without damaging the crystal can be a good parameter to know how much energy can be used. Nevertheless, multiphoton absorption can be a limiting factor.
- Vary the position of the grating and optimize the setup by moving both, the position of the crystal, and the position of the telescope.
- Vary the amount of negative chirp introduced to the pulse, and measure if there is an optimum point.

- At this moment the distance from the pump pulse to the setup has shown measurable fluctuations that can be avoided by moving the setup.

At this point we are waiting for some measurements that are done by our group to decide if further investigation can be done using cLT in PFT schemes. Parameters such as the absorption coefficient, transmission, and reflection of the crystal will be measured using TDS.

Chapter 4

Conclusion

4.1 Conclusion and remarks

In this thesis, we have presented a theoretical background about efficient THz generation by optical rectification using pulse front tilt schemes. In Chapter 2 we have experimentally investigated the most important tunable parameters in an efficient THz generation setup, and are:

- The use of cylindrical lenses to decouple tangential and sagittal focusing.
- Using the pulse duration as a tunable parameter, and introduce negative chirp to the pulse in order to maximize and fine-tune phase-matching.
- Cryo-cooling the crystal to reduce the linear absorption coefficient of the THz radiation.

In this experiment we report a record 2% efficiency available THz conversion efficiency, close to the maximum theoretical limit, and an excellent beam quality.

In Chapter 3 we have done a similar experiment, using pulse front tilt schemes with a cLT crystal pumped at $1\mu\text{m}$. This experiment has been done because cLT is a less studied, promising crystal that has the following advantages:

- The THz index of refraction of the Lithium Tantalate is higher than the one of Lithium Niobate.

- The damage threshold is higher than other materials such as: LN, ZnTe, or GaAs.

However, the obtained conversion efficiency is low. Measurements such as: transmission, and reflection coefficient are done by our group and depending on the obtained values further investigation using cLT will be done. Nevertheless, with the results obtained in Chapter 2 we grant electric fields as high as 0.2GV/m with 70 μ J energy, and beam focusable to nearly diffraction limit, specially suited for strong-field THz applications. More specifically, these specifications already suffice the requirements for a THz gun capable of accelerating electrons to several KeV range from rest.

Bibliography

- [1] NA Bannov, FT Vasko, and VV Mitin. Terahertz absorption by electrons and confined acoustic phonons in free-standing quantum wells. *Superlattices and microstructures*, 18(4):269, 1995.
- [2] Ariel Bruner, David Eger, Moshe B Oron, Pinhas Blau, Moti Katz, and Shlomo Ruschin. Temperature-dependent sellmeier equation for the refractive index of stoichiometric lithium tantalate. *Optics letters*, 28(3):194–196, 2003.
- [3] Anne-Laure Calendron, Hüseyin Çankaya, and Franz X Kärtner. High-energy khz yb: Kyw dual-crystal regenerative amplifier. *Optics express*, 22(20):24752–24762, 2014.
- [4] CFEL. Ultrafast optics and x-rays division, 2014.
- [5] B M Fischer, M Walther, and P Uhd Jepsen. Far-infrared vibrational modes of dna components studied by terahertz time-domain spectroscopy. *Physics in Medicine and Biology*, 47(21):3807, 2002.
- [6] B M Fischer, M Walther, and P Uhd Jepsen. Far-infrared vibrational modes of dna components studied by terahertz time-domain spectroscopy. *Physics in Medicine and Biology*, 47(21):3807, 2002.
- [7] J. A. Fülöp, L. Pálfalvi, S. Klingebiel, G. Almási, F. Krausz, S. Karsch, and J. Hebling. Generation of sub-mj terahertz pulses by optical rectification. *Opt. Lett.*, 37(4):557–559, Feb 2012.
- [8] József A Fülöp, Zoltán Ollmann, Csaba Lombosi, Christoph Skrobol, Sandro Klingebiel, László Pálfalvi, Ferenc Krausz, Stefan Karsch, and János Hebling. Efficient generation of thz pulses with 0.4 mj energy. In *CLEO: Science and Innovations*, pages SW1F–5. Optical Society of America, 2014.

-
- [9] József András Fülöp, László Pálfalvi, Matthias C. Hoffmann, and János Hebling. Towards generation of mj-level ultrashort thz pulses by optical rectification. *Opt. Express*, 19(16):15090–15097, Aug 2011.
- [10] Christoph P Hauri, Clemens Ruchert, Carlo Vicario, and Fernando Ardana. Strong-field single-cycle thz pulses generated in an organic crystal. *Applied Physics Letters*, 99(16):161116, 2011.
- [11] Janos Hebling, Gabor Almasi, Ida Kozma, and Jurgen Kuhl. Velocity matching by pulse front tilting for large area thz-pulse generation. *Optics Express*, 10(21):1161–1166, 2002.
- [12] Shu-Wei Huang, Eduardo Granados, Wenqian Ronny Huang, Kyung-Han Hong, Luis E. Zapata, and Franz X. Kärtner. High conversion efficiency, high energy terahertz pulses by optical rectification in cryogenically cooled lithium niobate. *Opt. Lett.*, 38(5):796–798, Mar 2013.
- [13] Jun ichi Shikata, Manabu Sato, Tetsuo Taniuchi, Hiromasa Ito, and Kodo Kawase. Enhancement of terahertz-wave output from linbo3 optical parametric oscillators by cryogenic cooling. *Opt. Lett.*, 24(4):202–204, Feb 1999.
- [14] G Kh Kitaeva. Terahertz generation by means of optical lasers. *Laser Physics Letters*, 5(8):559, 2008.
- [15] KA Kuznetsov, SP Kovalev, G Kh Kitaeva, TD Wang, YY Lin, YC Huang, II Naumova, and AN Penin. Dispersion of the dielectric function real part for mg: Linbo3 crystals at terahertz frequencies. *Applied Physics B*, 101(4):811–815, 2010.
- [16] Y.-S. Lee, T. Meade, M. DeCamp, T. B. Norris, and A. Galvanauskas. Temperature dependence of narrow-band terahertz generation from periodically poled lithium niobate. *Applied Physics Letters*, 77(9), 2000.
- [17] Mengkun Liu, Harold Y Hwang, Hu Tao, Andrew C Strikwerda, Kebin Fan, George R Keiser, Aaron J Sternbach, Kevin G West, Salinporn Kittiwatanakul, Jiwei Lu, et al. Terahertz-field-induced insulator-to-metal transition in vanadium dioxide metamaterial. *Nature*, 487(7407):345–348, 2012.

-
- [18] Emilio Alessandro Nanni, Wenqian Ronny Huang, Koustuban Ravi, Arya Fallahi, Gustavo Moriena, RJ Miller, and Franz X Kärtner. Terahertz-driven linear electron acceleration. *arXiv preprint arXiv:1411.4709*, 2014.
- [19] L Pálfalvi, JA Fülöp, Gy Tóth, and J Hebling. Evanescent-wave proton postaccelerator driven by intense thz pulse. *Physical Review Special Topics-Accelerators and Beams*, 17(3):031301, 2014.
- [20] L Pálfalvi, J Hebling, J Kuhl, A Peter, and K Polgár. Temperature dependence of the absorption and refraction of mg-doped congruent and stoichiometric linbo 3 in the thz range. *Journal of applied physics*, 97(12):123505–123505, 2005.
- [21] Koustuban Ravi, Wenqian Ronny Huang, Sergio Carbajo, Xiaojun Wu, and Franz Kärtner. Limitations to thz generation by optical rectification using tilted pulse fronts. *arXiv preprint arXiv:1406.1439*, 2014.
- [22] Arno Schneider, Max Neis, Marcel Stillhart, Blanca Ruiz, Rizwan UA Khan, and Peter Günter. Generation of terahertz pulses through optical rectification in organic dast crystals: theory and experiment. *JOSA B*, 23(9):1822–1835, 2006.
- [23] Mostafa Shalaby and Christoph P Hauri. Demonstration of a low-frequency three-dimensional terahertz bullet with extreme brightness. *Nature Communications*, 6, 2015.
- [24] H Tanoto, JH Teng, QY Wu, M Sun, ZN Chen, SA Maier, B Wang, CC Chum, GY Si, AJ Danner, et al. Greatly enhanced continuous-wave terahertz emission by nano-electrodes in a photoconductive photomixer. *Nature Photonics*, 6(2):121–126, 2012.
- [25] Masayoshi Tonouchi. Cutting-edge terahertz technology. *Nature photonics*, 1(2):97–105, 2007.
- [26] C Vicario, AV Ovchinnikov, SI Ashitkov, MB Agranat, VE Fortov, and CP Hauri. Generation of 0.9-mj thz pulses in dstms pumped by a cr: $\text{Mg}_i \text{sub}_i 2_i/\text{sub}_i \text{ sio}_i \text{sub}_i 4_i/\text{sub}_i$ laser. *Optics letters*, 39(23):6632–6635, 2014.
- [27] RS Weis and TK Gaylord. Lithium niobate: summary of physical properties and crystal structure. *Applied Physics A*, 37(4):191–203, 1985.

-
- [28] L Wimmer, G Herink, DR Solli, SV Yalunin, K Echterkamp, and C Ropers. Controlling and streaking nanotip photoemission by enhanced single-cycle terahertz pulses. *arXiv preprint arXiv:1307.2581*, 2013.
- [29] Zhang Xianbin, Li Yunfeng, Ma lijuan, Yuan ke, and Shi Wei. The impact of mgo-doped near-stoichiometric lithium niobate crystals on the thz wave output characteristics. *Journal of Physics: Conference Series*, 276(1):012226, 2011.
- [30] Guibao Xu, Xiaodong Mu, Yujie J. Ding, and Ioulia B. Zotova. Efficient generation of backward terahertz pulses from multiperiod periodically poled lithium niobate. *Opt. Lett.*, 34(7):995–997, Apr 2009.
- [31] Nan Ei Yu, Myoung-Kyu Oh, Hoonsoo Kang, Changsoo Jung, Bok Hyeon Kim, Kyu-Sup Lee, Do-Kyeong Ko, Shunji Takekawa, and Kenji Kitamura. Continuous tuning of a narrow-band terahertz wave in periodically poled stoichiometric lithium niobate crystal with a fan-out grating structure. *Applied Physics Express*, 7(1):012101, 2014.